Biosensors and Bioelectronics: X 18 (2024) 100475

Contents lists available at ScienceDirect

Biosensors and Bioelectronics: X

journal homepage: www.journals.elsevier.com/biosensors-and-bioelectronics-x

Folate receptors detection based on the immobilization of folic acid onto $Ti-W$ oxides thin film

Linda Bertel [a], Rogelio Ospina [a], José Miguel García-Martín [b], David A. Miranda [a,*]

[a] Universidad Industrial de Santander, Cra 27 Cll 9, Bucaramanga, 680002, Santander, Colombia
[b] Instituto de Micro y Nanotecnología, IMN-CNM, CSIC (CEI UAM+CSIC), Isaac Newton 8, E-28760, Tres Cantos, Madrid, Spain

ARTICLE INFO

Keywords:
Biosensor functionalization
Folic acid
Thin film
Electrochemical capacitance
Folate receptor

ABSTRACT

The overexpression of folate receptors on cell surfaces is associated with abnormalities linked to epithelial cancers. This study reports on a capacitive biosensor that employs folic acid as a recognition molecule for the biosensing of folate receptors. The biosensor is composed of a thin film of Ti–W oxides conjugated with folic acid that serves as a working electrode in a three-electrode electrochemical cell configuration. The thin film of Ti–W oxides, featuring a mixture of TiO_2 anatase and rutile phases, was fabricated using the pulsed laser deposition method and subsequently functionalized with folic acid. Characterization of the thin film before and after functionalization was conducted using AFM, XPS, and contact angle measurements. The functionalization study confirmed a stable bond between folic acid and the surface of the thin film. The interaction between the functionalized transducer and the folate receptor was investigated by determining the electrochemical capacitance using an electrochemical capacitance spectroscopy setup. Folate receptor recognition assays demonstrated that the biosensor response signal, or chemical hardness (in terms of electrochemical capacitance), is selective and directly proportional to the folate receptor concentration, with a limit of detection of 200 pM (0.2 nM). These findings are promising for the application of this detector in the recognition of folate receptors, particularly for point-of-care analysis.

1. Introduction

The folate receptor, a glycosylphosphatidylinositol-anchored cell surface receptor, is a notable cancer biomarker with a high affinity for folic acid (FA) molecules. FA, also known as vitamin B9, is vital for the synthesis of purines and thymidine and for the methylation of DNA, proteins, and lipids within the cell (Chen et al., 2013; Zwicke et al., 2012). Interestingly, FA retains its ability to bind to the folate receptor even after conjugation with drugs or diagnostic markers, enhancing its utility in targeted therapy and diagnostics (Zwicke et al., 2012). The functionalization of TiO_2 nanostructured surfaces with FA has led to the development of highly selective and sensitive folate receptor biosensors (Fan, Fan, Hu, Cui, Wang, Ma and Wei, 2020a). Furthermore, Venkatasubbu et al. successfully anchored FA to the surface of PEG-coated TiO_2 nanoparticles, facilitating targeted paclitaxel delivery to cancer cells (Devanand Venkatasubbu, Ramasamy, Ramakrishnan and Kumar, 2013).

In the past decade, the application of biosensors for cancer detection has gained considerable attention due to their high selectivity, precision, low cost, and rapid testing capabilities (Hasan et al., 2021).

Electrochemical biosensors that employ nanostructured TiO_2 surfaces as the working electrode are particularly appealing. These surfaces offer high biocompatibility, corrosion resistance, low manufacturing costs, high surface area, quantum confinement, efficient electronic charge properties, and strong adhesion to substrates (Bai and Zhou, 2014; Reghunath et al., 2021; Berger et al., 2012; Bertel et al., 2021). They have been used to assemble various biorecognition molecules, including antibodies, enzymes, or receptors (Bai and Zhou, 2014; Anaya-Esparza, Villagrán-de la Mora, Ruvalcaba-Gómez, Romero-Toledo, Sandoval-Contreras, Aguilera-Aguirre, Montalvo-González and Pérez-Larios, 2020; Reghunath et al., 2021; Mavrič et al., 2018).

The electrochemical behavior of TiO_2, extensively studied since its discovery, is fundamental to understanding and optimizing detection processes that involve charge generation, injection, separation, transport, or accumulation within the nanostructure (Berger et al., 2012; Bertel et al., 2021).

Among various electrochemical biosensors, those based on

* Corresponding author.
E-mail address: dalemir@uis.edu.co (D.A. Miranda).

https://doi.org/10.1016/j.biosx.2024.100475
Received 30 December 2023; Received in revised form 21 March 2024; Accepted 22 March 2024
Available online 2 April 2024

Electrochemical Capacitance Spectroscopy (ECS) are particularly intriguing. ECS-based capacitive biosensors, which use a redox-modified electrode and do not require the addition of a redox probe to the solution, represent a simpler alternative to traditional impedimetric biosensors (Santos, 2014).This allows a widerang eof combination so fbiorecognition elements/biomarkers, making the sesensors suitable for multiplexing applications with optimized frequencies (Fernandes et al., 2014; Bertel et al., 2021).

The use of mesoscopic structures for capacitive electrochemical detection is supported in the experimental measurement of electrochemical capacitance $C_{\overline{\mu}}$ (Corzo et al., 2021b; Pinzón et al., 2021); where capacitance $C_{\overline{\mu}}$ is defined as the variation of charge (q) with respect to the variation of the electric potential (φ), that is, $C_{\overline{\mu}} = dq/d\varphi$ (Bisquert, 2014; Bueno and Miranda, 2017). Using the concept of electrochemical potential $\overline{\mu} = \mu + q\varphi$, in terms of chemical potential μ and electric potential φ, simplifies the theoretical description of experimental measurement under potentiostatic conditions of an electrochemical biosensor. Taking into account a constant chemical potential (μ) and a specific temperature (T), and acknowledging that $q = zq_e$ (where q_e is the charge of an electron and z is the number of electrons that interact with φ), the chemical capacitance can be expressed as $C_{\overline{\mu}} = q_e z \partial q / \partial \overline{\mu}$, incorporating a partial derivative to denote the assumption of no variation of the chemical potential with changes in electrical potential. It is important to recognize that the charges present on the mesoscopic surface of the biosensor, q, can be modeled using the Fermi-Dirac distribution $\overline{n}_{FD}$, thus $q = q_e \overline{n}_{FD}$, where $\overline{n}_{FD} = [e^{(E-\overline{\mu})/k_B T} + 1]^{-1}$. Consequently, the chemical capacitance can be described by Eq. (1).

$$C_{\overline{\mu}} = q_e^2 z^2 \left(\frac{\partial \overline{n}_{FD}}{\partial \overline{\mu}}\right)_{\nu} = \frac{q_e^2 z^2}{k_B T} \overline{n}_{FD}(1 - \overline{n}_{FD}) \tag{1}$$

In this context, ν denotes the constant external thermodynamic potentials (Bueno and Miranda, 2017). For electrochemical biosensors, the total capacitance $C_{\overline{\mu}}$ is considered the series combination of the electrostatic capacitance C_e and the quantum capacitance C_q, following the relation $C_{\overline{\mu}}^{-1} = C_e^{-1} + C_q^{-1}$. Here, the (non-fradaic) C_e, also known as the ionic capacitance (Garrote et al., 2020), refers to Coulombic interactions. The most straightforward model to describe C_e is the capacitance of the electrochemical double layer; refer to the Supporting Information SI Fig. 1 (a). This capacitance characterizes polarized electrodes immersed in an electrolytic solution. The application of a specific potential to the electrode causes its surface to charge positively or negatively, attracting counterions and generating the electrochemical double-layer capacitance. This phenomenon, a measurable physical quantity, is highly sensitive to changes at the interface (Santos, 2014).

It is interesting to note that C_q has been identified as a faradaic contribution, which occurs specifically when a nanometric structure is charged, causing changes in the chemical potential (Santos, 2014; Bisquert, 2014). When a polarized metal-electrolyte interface, with its respective electrochemical double-layer capacitance, is modified with a molecular layer in the presence of a redox species, which can be faradaically charged, an additional element of charge is present, commonly called quantum capacitance in electrochemistry (C_q) (Santos, 2014); see a schematic detail in the Supporting Information SI Fig. 1(b). In this type of system, the magnitudes of the two contributions of $C_{\overline{\mu}}$ (C_e and C_q) are highly sensitive to the characteristics of the surface and the composition of the solution, and, in general, C_q is the predominant contribution (Santos, 2014). Experimentally, capacitance $C_{\overline{\mu}}$ is measured using ECS and is related to electrical impedance $Z(\omega)$ by $C^*(\omega) = [i\omega Z(\omega)]^{-1}$, where $\omega = 2\pi f$ represents the angular frequency and i is the imaginary unit $i = \sqrt{-1}$. The function $C^*(\omega)$ denotes a complex capacitance that can be decomposed into its real (C') and imaginary (C'') components, expressed as $C^*(\omega) = C' - iC''$. The capacitance $C_{\overline{\mu}}$ is then determined from the diameter of the semicircle in the capacitance spectrum in the Nyquist plot (Garrote et al., 2020).

For redox-active monolayers or nanometric structures, we can consider the approximation $C_e \gg C_q$, which leads to $C_{\overline{\mu}} \approx C_q$. Recently, it has been suggested that the inverse of $C_{\overline{\mu}}$ is an energy functional, in the framework of density functional theory (DFT) (Miranda and Bueno, 2016). This functional is directly associated with the chemical hardness at the interface, providing information on the reactivity and interaction dynamics of the system (Corzo et al., 2019; Miranda and Bueno, 2019). Chemical hardness, denoted η, is a critical parameter to assess chemical reactivity. It can be used experimentally to detect a target analyte employing an equation where γ represents a constant that encompasses the volume of the system, the square of the elementary charge and the oxidation state (Miranda and Bueno, 2016, 2019; Corzo et al., 2019, Corzo et al., 2021a).

$$\eta \approx \frac{\gamma}{C_{\overline{\mu}}} \tag{2}$$

The exploration of mesoscopic structures for capacitive electrochemical sensing signifies a leap towards innovative biosensing methodologies. This work presents advances in the functionalization of Ti–W oxide thin-film surfaces with FA molecules, achieving a covalent interaction essential for the detection of folate receptors. It underscores the potential of using electrochemical capacitance as a novel approach to detect cellular anomalies associated with cancer, particularly through the presence of folate receptors.

2. Methodology

2.1. $Ti - W$ oxides thin film deposition

Intrinsic Si wafers were cut into pieces measuring 2.2 cm by 1 cm. These substrates were cleaned with 2-propanol, followed by the placement of masks at one end of each sample, exposing 1.3 cm of substrate length for the deposition of oxides $Ti - W$.

Reactive pulsed laser deposition (PLD) was employed to fabricate the thin film. A metallic Ti–W target (10:90 wt%) rotating at 28 rpm was ablated using a third harmonic Nd: YAG laser at 355 nm. The laser beam, focused at a 45° angle onto the target, operated at a 10 Hz repetition rate with a pulse width of 6 ns and a fluence of 14.2 J/cm^2. The deposition chamber, made of stainless steel and evacuated by a turbo-molecular pump, achieved a base pressure of approximately 7×10^{-3} Pa $Ti - W$ oxides thin films were deposited at room temperature on semi-masked Si substrates (covering an area of 1.0 × 1.3 cm) from a target-substrate distance of 4.5 cm, in an oxygen atmosphere at 4.6 Pa for 5 min.

Following deposition, the masks were removed to reveal the Si regions that serve as electrical contacts for the biosensor.

2.2. Functionalization of $Ti - W$ oxides thin film with folic acid

Adapting the solvothermal strategy for modifying TiO_2 nanoparticles with carboxylic acids (Qu et al., 2010), a 2 mM folic acid (FA) solution was prepared in a 1:4 ethanol/water mixture, stirred on a magnetic plate for 5 min pH was adjusted between 10 and 11 by adding 1M NaOH dropwise. For XPS analysis, a higher FA concentration (50 mM) was used to ensure a detectable change in the N 1s signal. The FA solution, once heated to 54 °C, was used to immerse the thin film of $Ti - W$ oxide for 30 min, maintaining the temperature. After functionalization, the film was rinsed with type I water and dried with N_2 gas.

2.3. Characterization

The thickness of the thin film $Ti - W$ oxides was measured using AFM to image a step edge. Surface roughness and morphology before and after FA functionalization were examined by AFM (Hitachi Multifunction SPM Unit AFM5100N) in non-contact mode.

Raman spectroscopy (Horiba Scientific LabRam HR Evolution) assessed the thin film's structure using a 532 nm laser, a 600 lines/mm

grating, and a 100X long working distance objective, collecting spectra over 20 accumulations of 5 s each.

XPS analysis (SPECS surface characterization platform with a PHOIBOS 150 2D-DLD analyzer) was performed under 1×10^{-9} Pa, using a monochromatized Al $K\alpha$ source at 100 W, with pass energies set to 100 eV (broad spectra) and 20 eV (high-resolution spectra). Charge compensation was managed using a Flood Gun, with samples mounted on conductive tape and stainless steel holders. CasaXPS software, using Shirley background subtraction and RSF values for peak analysis, calibrated to C 1s at 284.6 eV, analyzed the spectra.

Contact angles were measured using the sessile drop technique with type I water and a KRÜSS DSA25E instrument, averaging measurements from at least three different locations per sample.

2.3.1. Electrochemical capacitance measurements

Measurements used a Metrohm Autolab PGSTAT-204 with an FRA-32M module in a three-electrode setup: the sample as the working electrode, a gold wire counter, and a Ag/AgCl reference electrode. A Faraday cage minimized external interference. Impedance spectra were recorded in PBS at the film's open-circuit potential, across 0.1 MHz to 0.1 Hz, with a 10 mV amplitude, averaging three replicates per condition. ECS data were analyzed by converting impedance to capacitance using the relation $C^*(\omega) = [i\omega Z(\omega)]^{-1}$, plotted as $C^{'}$ vs $C^{''}$ to model and extract parameters from the semicircular Nyquist plots.

2.3.2. Biosensor testing

Under sterile conditions, folate receptor solutions (0.1–26 nM in PBS) were prepared, with the biosensor incubated in each solution sequentially for 30 min, followed by washing and drying. ECS measurements before and after incubation provided capacitance spectra, from which the chemical hardness was calculated and fitted to a calibration curve for analyte detection. Controls included non-functionalized $Ti-W$ oxide films and specificity tests against fetal bovine serum, assessing interference and biosensor selectivity.

$$R(\%) = \frac{C_{\bar{\mu}} - C_{\bar{\mu},0}}{C_{\bar{\mu},0}} \times 100 \tag{3}$$

3. Results and discussion

3.1. $Ti-W$ oxides thin film

The deposition of $Ti-W$ oxides resulted in a thin film approximately 6 nm thick, achieved at a laser fluence of 14.2 Jcm^{-2}. Representative AFM images, depicted in Fig. 1, illustrate the surface of the thin film of oxides $Ti-W$. Raman spectroscopy confirms the presence of characteristic bands of the anatase and rutile phases of TiO_2 at 147 cm^{-1} and 233, 433, 620, and 822 cm^{-1}, respectively (see SI Fig. 2 in Supporting Information), indicating the mixed phase composition of the thin film (Su et al., 2008; Mondal et al., 2013). Additional bands at 300 cm^{-1} and 520 cm^{-1} are attributed to Si–Si vibrations from the substrate, while a band around 950 cm^{-1} suggests Si–O–Ti interactions (Subramanian et al., 2008).

We confirmed the presence of adsorbed oxygen species, double carbon bonds, and hydroxyl groups in the $Ti-W$ oxide thin film through high resolution XPS spectra of O 1, as shown in Supplementary Information SI Fig. 3(A). A peak at 533.6 eV is associated with adsorbed oxygen species (Hu et al., 2016), while the peak at 531.9 eV corresponds to surface hydroxyl groups (OH) and/or C═O bonds (Gao et al., 2017; Zamharir et al., 2014). The peak at 530.4 eV is attributed to lattice oxygen bound to W and Ti (Gao et al., 2017; Vargas et al., 2015), indicating exposure of the thin film to ambient conditions. Furthermore, the Ti 2p spectrum of the thin film of fabricated oxide $Ti-W$, presented in Supplementary Fig. 3B, shows two characteristic peaks of Ti(IV) in TiO_2 at 458.7 and 464.6 eV, closely aligned with the values of the literature (Biesinger et al., 2010).

Furthermore, we confirmed the presence of oxidized states by analyzing the high-resolution XPS spectrum of the thin oxide film $Ti-W$ for W 4f, as illustrated in the SI Supplementary Information SI Fig. 3(C). Two peaks located at 37.9 and 35.8 eV were identified, corresponding to the $W\,4f_{5/2}$ and $W\,4f_{7/2}$ signals, respectively (Riboni et al., 2013). The position and shape of these peaks are indicative of W atoms in an oxidation state of +6, consistent with the expected composition of $W\,O_3$ (Vasilopoulou et al., 2014).

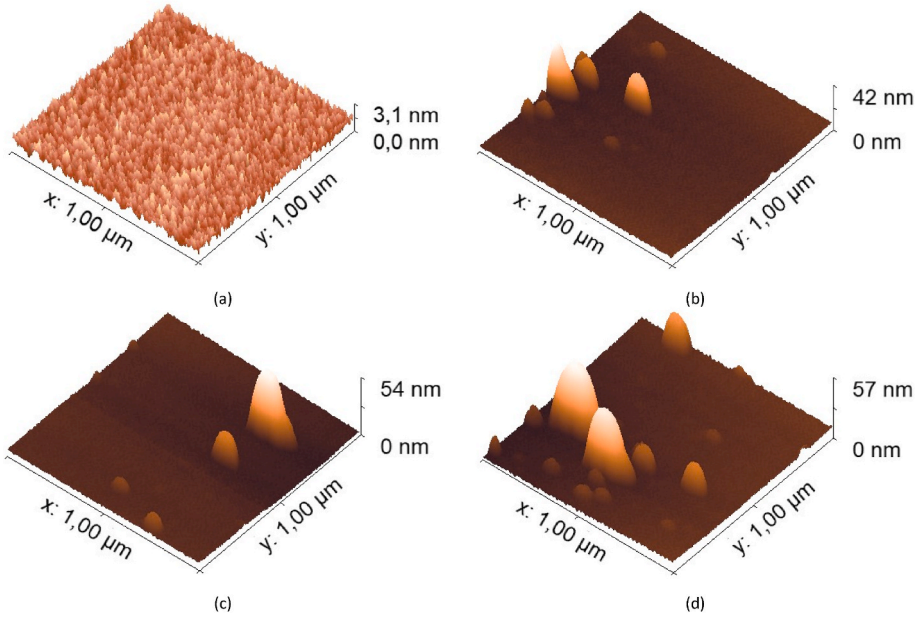

Fig. 1. AFM images of (a) a $Ti-W$ oxides thin film and different regions of the FA-functionalized $Ti-W$ oxides thin film with RMS roughness of (b) 2.9, (c) 5 and (d) 7.8 nm.

3.2. FA-functionalized Ti – W oxides thin film

The topography of the thin film *Ti – W* oxides before and after FA functionalization was studied by AFM image analysis. In Fig. 1 (a) the homogeneity of a pristine *Ti – W* oxide thin film can be observed, with a RMS roughness of 0.4 nm. However, after the functionalization process of this film, the morphology changes dramatically; see Fig. 1: large dots appear, with height that reaches tens of nm in some cases, and therefore the RMS roughness increases to 2.9, 5 and 7.8 nm in the three areas scanned in Fig. 1 (a), (b) and (c), respectively. Such dots can be ascribed to the presence of FA-molecule aggregates.

High-resolution C 1s and N 1s XPS spectra are presented in Fig. 2 for both the pristine and FA functionalized *Ti – W* oxide thin films, along with FA itself. In Fig. 2(a), the C 1s spectrum of the pristine oxide thin film *Ti – W* reveals peaks at 284.6, 286.1, and 288.3 eV. These are attributed to organic environmental contaminants, corresponding to C–C/C═C, C═O (or C–N) and O═C–O configurations, respectively, following the assignments by (Zhao et al., 2017; Wang et al., 2015). On the contrary, the FA-functionalized film's C 1s spectrum, illustrated in Fig. 2(b), clearly shows a peak at 287.8 eV, indicative of the C═O/C–N group specific to FA (Zhao et al., 2017; Wang et al., 2015). Remarkably, the 288.4 eV peak, typically associated with organic contaminants, is absent in the functionalized film spectrum. This observation suggests that the incorporation of FA displaces these contaminants or facilitates their removal during the functionalization process (Gomes, Azevedo Neto, Bronze-Uhle, Trino, dos Santos, da Silva and Lisboa-Filho, 2019).

The N 1s spectrum of the FA-functionalized *Ti – W* oxides thin film, see Fig. 2 (e), presents a signal with two contributions at 399.2 and 398.8 eV, just like in the FA spectra, due to the C═N and C–N groups (Wang et al., 2018) respectively. The N 1s spectrum of the thin film *Ti – W* oxides shows a small signal that may be due to nitrogen-containing molecules from ambient conditions that were physisorbed in the sample, in agreement with the signal due to C–N bonds (at 286.1 or 286.6 eV) in both the C 1s spectrum of the thin film of *Ti – W* oxides and that of the thin film of FA functionalized oxides *Ti – W*. These observations obtained from the XPS analyzes indicate that FA was bound to the surface of the *Ti – W* oxides, probably through the carboxylic groups of the Glu moiety, leaving the pteridine moiety free.

Qu et al. suggest that p-bromobenzoic acid binds to the surface of TiO_2 nanoparticles through two key steps: 1) the formation of double hydrogen bonds between p-bromobenzoic acid and *TiO*2 at the same site of Ti and 2) coordination at solvothermal temperature by dehydration of

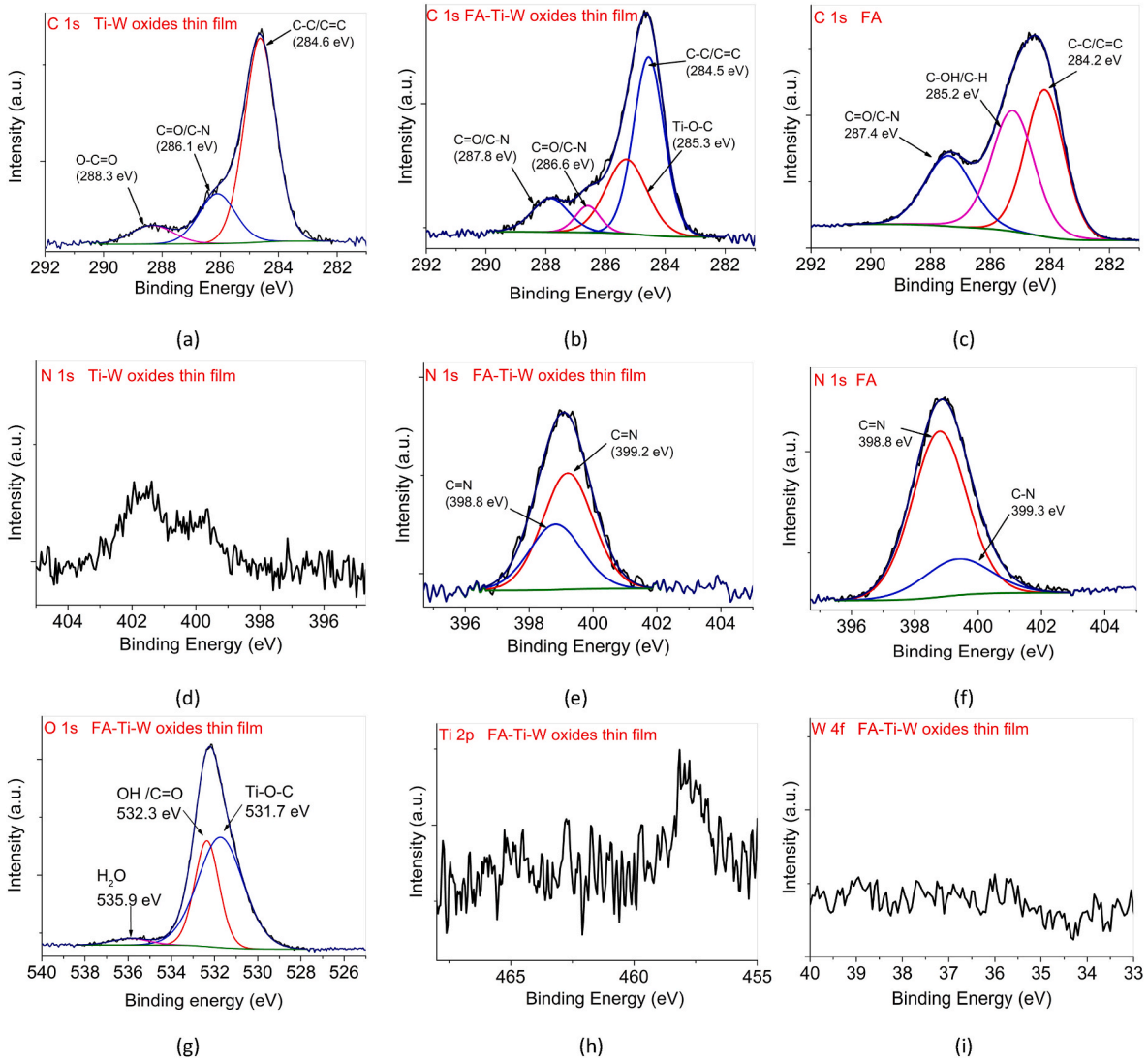

Fig. 2. High-resolution XPS spectra: C 1s spectra of (a) the pristine thin film, (b) the FA-functionalized thin film, and (c) FA itself; N 1s spectra of (d) the pristine thin film, (e) the FA-functionalized thin film, and (f) FA; O 1s spectrum of (g) the FA-functionalized thin film; and Ti 2p (h) and W 4f (i) spectra of the FA-functionalized thin film.

the hydrogen bonds (Qu et al., 2010). In this sense, a binding mechanism of FA to the $Ti-W$ oxide surface similar to that presented by Qu et al. is proposed; see mor details in the Supporting Information SI Fig. 4.

Additional evidence of the covalent bond between the $Ti-W$ oxide thin film and FA through the carboxylic group of FA includes the presence of peaks at 287.8 eV and 285.3 eV in the C 1s XPS spectra of the FA-functionalized thin film, as shown in Fig. 2(b). The peak at 287.8 eV, associated with C═O groups (Zhao et al., 2017), aligns with the signal observed for free FA at 287.4 eV, indicating the presence of FA on the surface of the film. The peak at 285.3 eV is attributed to Ti–O–C (Xing et al., 2014), which confirms the formation of a covalent bond between FA and the oxide surface. The existence of Ti–O–C bonds is further corroborated by a peak at 531.7 eV in the high-resolution O 1s XPS spectrum of the FA-functionalized film (Fig. 2(g)). Additionally, the O 1s spectrum reveals two other signals: one at 532.3 eV, related to surface hydroxyl groups or C═O bonds (Gao et al., 2017; Zamharir et al., 2014), and another at 535.9 eV, possibly attributed to physisorbed water (Benko et al., 2015).

In the case of FA-functionalized $Ti-W$ oxides thin film, the high resolution spectrum of XPS for Ti 2p showed a decrease in resolution of the two peaks; see Fig. 2 (h). However, in the W 4f spectrum of the thin film of FAfunctionalized $Ti-W$ oxides, the two peaks corresponding to $W\,4f_{5/2}$ and $W\,4f_{7/2}$ are not observed (Fig. 2 (i)). These results for the Ti 2p and W 4f spectra may indicate that the FA molecules have covered the film surface to a large extent, leaving the Ti and W atoms covered and therefore the resolution of these two elements is reduced.

Furthermore, the binding of FA to the surface of the thin film of oxides $Ti-W$ was verified by analyzing the contact angle of the thin film of oxides $Ti-W$ before and after functionalization, which is presented in SI Fig. 5. The contact angle of the functionalized film was reduced to less than half the contact angle of the thin film of oxides $Ti-W$, indicating the increased hydrophilicity of the film due to free amine ($-NH_2$) and carboxylic acid ($-COOH$) of FA.

3.3. Capacitive response to folate receptors binding

The thin film of $Ti-W$ oxide was functionalized with FA to endow it with the ability to recognize folate receptors on its surface. The interaction of the thin FA functionalized oxide film $Ti-W$ with various concentrations of folate receptors, followed by an analysis of the capacitive spectra, showed that the electrochemical capacitance, $C_{\bar{\mu}}$, of the film decreases as the analyte concentration increases. Detailed observations are documented in the Supplementary Information SI Fig. 6. This trend corroborates the findings of previous studies involving different analytes, validating this approach for the determination of $C_{\bar{\mu}}$ (Corzo et al., 2021a; Lehr et al., 2014). To elucidate this phenomenon, we refer to the circuit model proposed by Corzo et al. (2021a), adapted for our context in the Supplementary Information SI Fig. 7. A critical insight from this adapted model is that the number of active sites decreases as the folate receptors bind to the FA on the surface of the biosensor, indicating a direct interaction that affects the capacitive properties of the sensor.

Further processing of the experimental data yields the calibration curve depicted in Fig. 3 (a). Here, the sensor signal $S([X])$, influenced by the chemical hardness η and expressed through Eq. (4), correlates with the concentration of the folate receptor, $[X]$. Importantly, η_0 and $C_{\bar{\mu},0}$ represent the baseline values of the chemical hardness (Miranda and Bueno, 2019) and electrochemical capacitance, respectively, before the introduction of the analyte.

$$S([X]) = \frac{\eta([X])}{\gamma} - \frac{\eta_0}{\gamma} = \frac{1}{C_{\bar{\mu}}([X])} - \frac{1}{C_{\bar{\mu},0}} \tag{4}$$

A linear response was observed for the FA-functionalized $Ti-W$ oxide thin film in the detection of folate receptors, as demonstrated by plotting the measurement signal S, derived from Eq. (4), against the receptor concentration. In this analysis, $C_{\bar{\mu}}$ was normalized to the detector surface area. Furthermore, the Limits of Detection (LoD) and Quantification (LoQ) were determined to be 200 pM (or 0.2 nM) and 700 pM (or 0.7 nM), respectively, showcasing the promising potential of this detection method. These values are in agreement with those reported for other detectors that employ $C_{\bar{\mu}}$ for the detection of analytes (Fernandes et al., 2014). Although not reaching the sensitivity levels of 5.3 fM and 1.69 pM achieved by Fan et al. and Geetha et al. in the electrochemical detection of folate receptors (Fan, Fan, Hu, Cui, Wang, Ma and Wei, 2020b; Geetha Bai, Muthoosamy, Tuvikene, Nay Ming and Manickam, 2021), simplicity, cost effectiveness and suitability for Point of Care (PoC) testing by non-specialists make the proposed biosensor a valuable tool.

To assess the capability of the biosensing system to quantify the molecular binding affinity constant (K_a) between FA (anchored to the $Ti-W$ oxide thin film) and folate receptors, we applied the Langmuir adsorption isotherm model. This model distinguishes two scenarios: i) unoccupied FA sites (A) and ii) FA receptor complexes (AX). The equilibrium between unbound FA sites and their interaction with folate receptors is given by $A + X \rightleftharpoons AX$, leading to the definition of K_a as $K_a = [AX]/([A][X])$ (Fernandes et al., 2014), where [ ] denotes

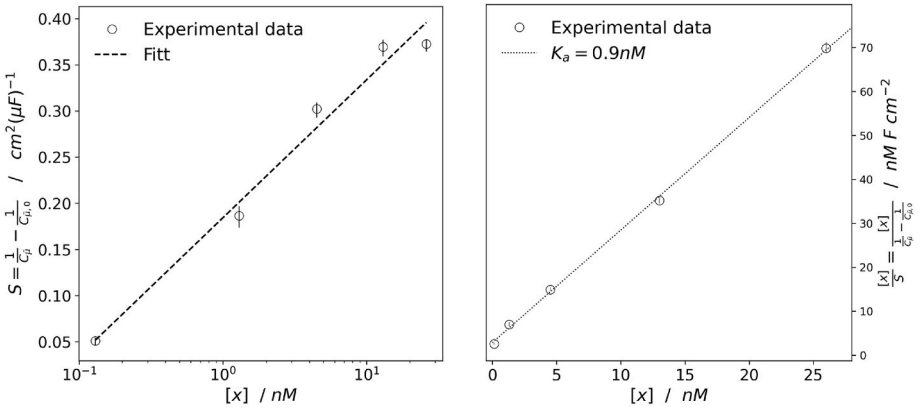

Fig. 3. Calibration curves for the detection of folate receptors: (a) utilizing chemical hardness as the response signal ($S = C_{\bar{\mu}}^{-1} - C_{\bar{\mu},0}^{-1}$ plotted against folate receptor concentration $[X]$), and (b) fitting the data to the Langmuir model ($[X]S^{-1}$ versus $[X]$). Each point represents the mean of three measurements, with the dotted line depicting the best fit. The relative standard deviations (RSD) for folate receptor concentrations ranging from 0.13 to 26 nM were 5.97%, 2.67%, 2.36%, 1.74%, and 1.10%, respectively.

concentration. Assuming surface coverage $\boldsymbol{\theta}$ and available sites as $1-\boldsymbol{\theta}$, the expression for K_a can be transformed into $K_a[X] = \theta/(1-\theta)$. Solving for $\boldsymbol{\theta}$ yields $\theta = K_a[X]/(1+K_a[X])$. Biomolecular surface coverage, Γ (in $mol\ cm^{-2}$), is directly correlated with $\boldsymbol{\theta}$, suggesting $\Gamma = \boldsymbol{\theta}\Gamma_m$, where Γ_m is the maximum adsorption at complete surface coverage, leading to $\Gamma = \Gamma_m K_a[X]/(1+K_a[X])$. This relationship can be linearized as shown in Eq. (5).

$$\frac{[X]}{\Gamma} = \frac{[X]}{\Gamma_m} + \frac{1}{K_a\Gamma_m} \tag{5}$$

Considering that an increase in Γ corresponds to an increase in the measurement signal S, Eq. (5) can be reformulated as Eq. (6), where $S = C_{\bar{\mu}}^{-1} - C_{\bar{\mu},0}^{-1}$, with $C_{\bar{\mu}}$ representing the electrochemical capacitance at a specific concentration of analytes, and $C_{\bar{\mu},0}$ denoting the capacitance of the blank interface. S_m is the sensor response at maximum adsorption.

$$\frac{[X]}{S} = \frac{[X]}{S_m} + \frac{1}{K_a S_m} \tag{6}$$

A K_a value of $0.9\,nM$ was determined, indicating that the experimental data align well with the model ($y = mx + b$) when plotting $[X]S^{-1}$ against $[X]$, as shown in Fig. 3. Given that $K_a \approx 1.0\,nM$ (Devanand Venkatasubbu et al., 2013), we infer that the detection mechanism specifically involves the interaction between FA and the folate receptor.

In a control experiment evaluating the $Ti-W$ oxide thin film without FA functionalization for the detection of the folate receptor, we observed that the electrochemical capacitance $C_{\bar{\mu}}$ of the film did not vary with the concentration of the folate receptor, indicating a lack of inherent sensing capability. This observation is detailed in Table 1, which lists the $C_{\bar{\mu}}$ values for both blank measurements (the thin oxide film $Ti-W$ incubated with PBS for 30 min) and measurements at different folate receptor concentrations. In particular, $C_{\bar{\mu}}$ showed minimal variation, with an average value of $2.74\,\mu Fcm^{-2}$ and a standard deviation of $0.03\,\mu Fcm^{-2}$. This stability in $C_{\bar{\mu}}$ values underscores the specificity of the FA-functionalized $Ti-W$ oxide thin film toward folate receptors, as further evidenced by the experimental data in Supplementary Information SI Fig. 6.

Lastly, to assess the response of the proposed detector to potential interferences, we evaluated its selectivity using Fetal Bovine Serum (FBS), known for its complex protein composition similar to that of biological samples from real patients. The response of $C_{\bar{\mu}}$ to FBS produced a modest increase of 4.30%, reflecting serum protein concentrations in the range of micro molar. This stark difference in response underscores the selective affinity of the FA-functionalized $Ti-W$ oxide thin film for folate receptors, highlighting its potential for specific biosensing applications.

4. Conclusions

We have developed a biosensor for the detection of folate receptors, using a thin film of oxide $Ti-W$ functionalized with folic acid. The covalent binding of the carboxylic groups of folic acid to the thin film is critical to the specificity of the biosensor and its ability to operate on the basis of the affinity of this interaction. Characterization efforts have confirmed the nanomolar detection and quantification limits of the biosensor, emphasizing its high sensitivity and potential for point-of-care applications. The experimentally determined biochemical affinity correlates with theoretical models for the interaction of folic acid and folate receptors, which confirms the functionality of the biosensor.

Future work will focus on exploring various nanostructures of TiO_2 and $Ti-W$ oxides to potentially achieve $C_{\bar{\mu}}$ values on the order of $10^2\,\mu Fcm^{-2}$. Advances in this area could significantly enhance the performance of the biosensor, leading to even lower detection limits and broadening the range of its applicability in clinical diagnostics. This study lays the foundation for the continued development of highly sensitive detection methods for folate receptors and potentially other biomarkers.

Table 1
$C_{\bar{\mu}}$ values obtained when a $Ti-W$ oxide thin film was used as a working electrode for the measurement of blank and different concentrations of folate receptors with Relative standard deviations (RSD).

Measurement number of $C_{\bar{\mu}}$ [μFcm^{-2}]	Blank	0.1 nM	1.3 nM	4.5 nM	13 nM	26 nM
1	2.68	2.75	2.73	2.76	2.74	2.76
2	2.68	2.74	2.73	2.75	2.74	2.75
3	2.69	2.75	2.73	2.76	2.74	2.76
RSD [%]	0.14	0.14	0.08	0.27	0.08	0.13

CRediT authorship contribution statement

Linda Bertel: Writing – review & editing, Writing – original draft, Visualization, Validation, Methodology, Investigation, Formal analysis, Data curation, Conceptualization. **Rogelio Ospina:** Writing – review & editing, Supervision, Methodology, Investigation, Conceptualization. **José Miguel García-Martín:** Writing – review & editing, Supervision, Resources, Project administration, Investigation, Funding acquisition, Formal analysis, Conceptualization. **David A. Miranda:** Writing – review & editing, Supervision, Software, Resources, Project administration, Methodology, Investigation, Funding acquisition, Formal analysis, Data curation, Conceptualization.

Declaration of competing interest

The authors declare that they have no known competing financial interests or personal relationships that could have appeared to influence the work reported in this paper.

Data availability

Data will be made available on request.

Acknowledgments

This research was supported by the I–COOP+2018 program of CSIC (ref. COOPA20305) and the *Universidad Industrial de Santander* (VIE 2816). We express our gratitude to the teams at the *Laboratorio de Ciencia de Superficies* and the *Laboratorio de Espectroscopa* at the *Parque Tecnológico de Guatiguará*, *University Industrial de Santander*, for their invaluable assistance with the XPS and Raman analyses.

Appendix A. Supplementary data

Supplementary data to this article can be found online at https://doi.org/10.1016/j.biosx.2024.100475.

References

Anaya-Esparza, L.M., Villagrán-de la Mora, Z., Ruvalcaba-Gómez, J.M., Romero-Toledo, R., Sandoval-Contreras, T., Aguilera-Aguirre, S., Montalvo-González, E., Pérez-Larios, A., 2020. Processes 8.
Bai, J., Zhou, B., 2014. Chem. Rev. 114, 10131–10176.
Benko, A., Frączek-Szczypta, A., Menaszek, E., Wyrwa, J., Nocuń, M., Błażewicz, M., 2015. J. Mater. Sci. Mater. Med. 26, 262.
Berger, T., Monllor-Satoca, D., Jankulovska, M., Lana-Villarreal, T., Gómez, R., 2012. ChemPhysChem 13, 2824–2875.
Bertel, L., Miranda, D.A., García-Martín, J.M., 2021. Sensors 21.
Biesinger, M.C., Lau, L.W.M., Gerson, A.R., St, R., Smart, C., 2010. Appl. Surf. Sci. 257, 887–898.
Bisquert, J., 2014. Nanostructured Energy Devices. CRC Press.
Bueno, P.R., Miranda, D.A., 2017. Phys. Chem. Chem. Phys. 19, 6184–6195.
Chen, C., Ke, J., Zhou, X.E., Yi, W., Brunzelle, J.S., Li, J., Yong, E.L., Xu, H.E., Melcher, K., 2013. Nature 500, 486–489.
Corzo, S.P., Bueno, P.R., Miranda, D.A., 2019. The experimental chemical hardness in the interaction between β-tubulin and epothilone B. J. Phys. Conf. 1403, 012016. https://doi.org/10.1088/1742-6596/1403/1/012016.

Corzo, S.P., Bueno, P.R., Miranda, D.A., 2021a. IEEE Access 9, 166446–166454.
Corzo, Sandra P., Bueno, Paulo R., Miranda, David A., 2021b. Improving the Analytical Reproducibility of Electrochemical Capacitive Sensors Using the Chemical Hardness of the Interface. IEEE. https://doi.org/10.1109/ACCESS.2021.3135787.
Devanand Venkatasubbu, G., Ramasamy, S., Ramakrishnan, V., Kumar, J., 2013. Adv. Powder Technol. 24, 947–954.
Fan, B., Fan, Q., Hu, L., Cui, M., Wang, X., Ma, H., Wei, Q., 2020a. ACS Appl. Mater. Interfaces 12, 1877–1884. PMID: 31816239.
Fan, B., Fan, Q., Hu, L., Cui, M., Wang, X., Ma, H., Wei, Q., 2020b. ACS Appl. Mater. Interfaces 12, 1877–1884. PMID: 31816239.
Fernandes, F.C., Santos, A., Martins, D.C., Góes, M.S., Bueno, P.R., 2014. Biosens. Bioelectron. 57, 96–102.
Gao, L., Gan, W., Qiu, Z., Zhan, X., Qiang, T., Li, J., 2017. Sci. Rep. 7, 1102.
Garrote, B.L., Santos, A., Bueno, P.R., 2020. Nat. Protoc. 15, 3879–3893.
Geetha Bai, R., Muthoosamy, K., Tuvikene, R., Nay Ming, H., Manickam, S., 2021. Nanomaterials 11.
Gomes, O.P., Azevedo Neto, N.F., Bronze-Uhle, E.S., Trino, L.D., dos Santos, C.M., da Silva, J.H., Lisboa-Filho, P.N., 2019. Mater. Chem. Phys. 223, 32–38.
Hasan, M., Ahommed, M., Daizy, M., Bacchu, M., Ali, M., Al-Mamun, M., Saad Aly, M., Khan, M., Hossain, S., 2021. Biosens. Bioelectron. X 8, 100075.
Hu, J., Wang, L., Zhang, P., Liang, C., Shao, G., 2016. J. Power Sources 328, 28–36.
Lehr, J., Fernandes, F.C.B., Bueno, P.R., Davis, J.J., 2014. Anal. Chem. 86, 2559–2564. PMID: 24491045.
Mavrič, T., Benčina, M., Imani, R., Junkar, I., Valant, M., Kralj-Iglič, V., Iglič, A., 2018. Chapter three - electrochemical biosensor based on tio2 nanomaterials for cancer diagnostics. Academic Press. Volume 27 of *Advances In Biomembranes And Lipid Self-Assembly*, pp. 63–105.
Miranda, D.A., Bueno, P.R., 2016. Phys. Chem. Chem. Phys. 18, 25984–25992.
Miranda, D.A., Bueno, P.R., 2019. J. Phys. Chem. C 123, 21213–21223.
Mondal, A., Dhar, J.C., Chinnamuthu, P., Singh, N.K., Chattopadhyay, K.K., Das, S.K., Das, S.C., Bhattacharyya, A., 2013. Electron. Mater. Lett. 9, 213–217.
Pinzón, E.F., Santos, A.d., Bueno, P.R., 2021. ACS Appl. Electron. Mater. 3, 3411–3417.
Qu, Q., Geng, H., Peng, R., Cui, Q., Gu, X., Li, F., Wang, M., 2010. Langmuir 26, 9539–9546. PMID: 20345108.
Reghunath, S., Pinheiro, D., Kr, S.D., 2021. Appl. Surf. Sci. Advan. 3, 100063.
Riboni, F., Bettini, L.G., Bahnemann, D.W., Selli, E., 2013. Catal. Today 209, 28–34.
Santos, A., 2014. J. Anal. Bioanal. Tech. S7.
Su, W., Zhang, J., Feng, Z., Chen, T., Ying, P., Li, C., 2008. J. Phys. Chem. C 112, 7710–7716.
Subramanian, M., Vijayalakshmi, S., Venkataraj, S., Jayavel, R., 2008. Thin Solid Films 516, 3776–3782.
Vargas, M., Lopez, D., Murphy, N., Grant, J., Ramana, C., 2015. Appl. Surf. Sci. 353, 728–734.
Vasilopoulou, M., Soultati, A., Georgiadou, D.G., Stergiopoulos, T., Palilis, L.C., Kennou, S., Stathopoulos, N.A., Davazoglou, D., Argitis, P., 2014. J. Mater. Chem. A 2, 1738–1749.
Wang, Q., Zhang, Q., Chen, Y., He, J., Jiang, K., Hu, Z., Zhong, X., 2018. Plasma Process. Polym. 15, 1700088.
Wang, Y., Zhang, C., Li, H., Zhu, G., Bao, S.S., Wei, S., Zheng, L.M., Ren, M., Xu, Z., 2015. J. Mater. Chem. B 3, 296–305.
Xing, M., Shen, F., Qiu, B., Zhang, J., 2014. Sci. Rep. 4, 6341.
Zamharir, S.G., Ranjbar, M., Salamati, H., 2014. Sol. Energy Mater. Sol. Cell. 130, 27–35.
Zhao, X., Zhang, J., Shi, L., Xian, M., Dong, C., Shuang, S., 2017. RSC Adv. 7, 42159–42167.
Zwicke, G.L., Mansoori, G.A., Jeffery, C.J., 2012. Nano Rev. 3, 18496. PMID: 23240070.